Chemical Engineering Journal 369 (2019) 223–232

Contents lists available at ScienceDirect

Chemical Engineering Journal

journal homepage: www.elsevier.com/locate/cej

Metal-free graphene-based catalytic membrane for degradation of organic contaminants by persulfate activation

Marta Pedrosa[a], Goran Drazic[b], Pedro B. Tavares[c], José L. Figueiredo[a], Adrián M.T. Silva[a,*]

[a] Laboratory of Separation and Reaction Engineering, Laboratory of Catalysis and Materials (LSRE-LCM), Faculdade de Engenharia, Universidade do Porto, Rua Dr. Roberto Frias, 4200-465 Porto, Portugal

[b] Department for Materials Chemistry, National Institute of Chemistry, Hajdrihova 19, SI-1000 Ljubljana, Slovenia

[c] Centro de Química–Vila Real, Universidade de Trás-os-Montes e Alto Douro, Departamento de Química, Vila Real 5000-801, Portugal

HIGHLIGHTS

- N-doped graphene oxide (GO) samples were prepared with different N precursors.
- A metal-free N-doped GO membrane was also developed.
- The treatment of organic pollutants by persulfate (PS) activation was investigated.
- Using the membrane, instead of powders, avoids the catalyst separation step.
- Loss of N-pyridinic groups decreases the membrane catalytic activity.

GRAPHICAL ABSTRACT

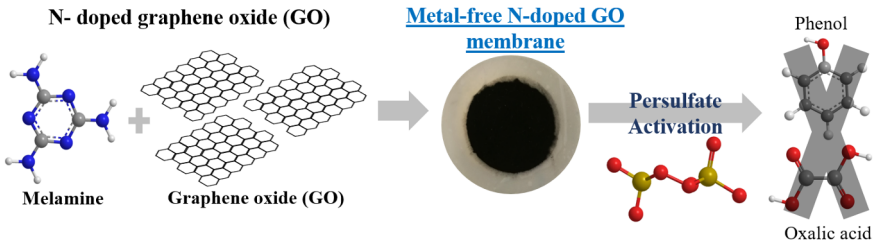

ARTICLE INFO

Keywords:
Metal-free membrane
N-doped graphene oxide
Persulfate activation
Wastewater treatment
Organic pollutants
Advanced oxidation processes (AOPs)

ABSTRACT

The persulfate (PS) activation can be successfully applied in water treatment and the use of carbon materials to activate PS has been thoroughly described in the literature. Nevertheless, the prospect of employing a metal-free catalytic membrane as the single activator of PS has to be better studied. In the present work, graphite oxide was prepared by the modified Hummers' method and different nitrogen precursors (melamine, urea and gaseous ammonia) were investigated to produce N-doped graphene oxide catalysts. The material prepared with melamine presented the highest nitrogen content (23.78 wt%) and the highest catalytic activity for the degradation of phenol in aqueous solution. The membrane fabricated with this catalyst was applied in filtration experiments for the degradation of phenol and oxalic acid. The catalytic mechanism is governed by both the radical and the non-radical degradation of the pollutants, but a more notorious contribution of singlet oxygen species was observed. It was demonstrated that the membrane lost the N-pyridinic groups during the reaction and, as consequence, part of its catalytic activity, whereas N-quaternary species remained in the used membrane. An important advantage associated with the application of this metal-free catalytic membrane, instead of a catalyst in powder form, is to avoid the final catalyst separation step.

1. Introduction

Water treatment is a research subject of wide interest, given the universal importance of clean water. Advanced oxidation processes (AOPs) can be successfully applied for water treatment and are mainly focused on the generation of hydroxyl radicals ($HO^{\cdot}$) to oxidize the

* Corresponding author.
E-mail address: adrian@fe.up.pt (A.M.T. Silva).

https://doi.org/10.1016/j.cej.2019.02.211
Received 13 October 2018; Received in revised form 6 February 2019; Accepted 28 February 2019
Available online 01 March 2019

Table 1
Fabricated catalytic materials.

Material	Procedure
rGO-A	Graphite oxide treated in a furnace up to 500 °C under 10:90% NH_3:N_2 atmosphere, for 10 min [12]
rGO-U	Graphite oxide and 0.6 g of urea were dispersed in ethanol and the liquid was evaporated. The powder was treated in a muffle furnace at 350 °C, under air atmosphere, for 30 min [13]
rGO-M (0.4)*	Graphite oxide and 0.4 g of melamine were dispersed in ethanol and the liquid was evaporated. The powder was treated in a muffle furnace at 350 °C, under air atmosphere, for 30 min [13]
rGO	The same procedure [13] was employed without nitrogen precursors (i.e., a partially reduced GO sample is obtained)

*Materials with other amounts of melamine (0.2, 0.8 and 1.6 g) were also prepared by this procedure (rGO-M (0.2), rGO-M (0.8) and rGO-M (1.6), respectively).

organic pollutants. On the other hand, sulfate radical ($SO_4^{\cdot -}$) based processes have shown significant advantages over conventional AOPs, since $SO_4^{\cdot -}$ has a high redox potential (2.5–3.1 V), long half-life (30–40 μs), it reacts with organic compounds in a wide range of pH values as well as with water or hydroxide ions to produce $HO^{\cdot}$ radicals [1–3]. $SO_4^{\cdot -}$ can react with the organic compounds by hydrogen abstraction; electron transfer donating substituents; and addition reactions with unsaturated bonds [1,4]. Peroxymonosulfate (PMS) and persulfate (PS) are the most widely employed precursors of $SO_4^{\cdot -}$, sodium persulfate ($Na_2S_2O_8$) being preferred for water treatment applications, as it is very soluble and stable [1].

There are many approaches to activate the production of $SO_4^{\cdot -}$, such as light irradiation, ultrasounds, temperature, microwaves and metal or non-metal catalysts [1]. At an industrial level, metal catalysts are used for a variety of applications, which implicates high costs, both economically and environmentally. Thus, new research for non-metal catalysts is crucial. Here, carbon materials appear as a good alternative to traditional metals. In carbocatalysis, the active sites for metal-free oxidation of contaminants with PS or PMS can be the sp^2 carbon, zigzag edges and electron-rich surface oxides (i.e. carboxyl and carbonyl groups) [1,5,6].

Among the vast assortment of carbon materials, graphene oxide (GO) derivatives stand out, due to the fine-tuning potential of their structure, making them suitable candidates for PS and PMS activation in catalysis [1,7,8]. The first report on the use of reduced graphene oxide (rGO) to activate PMS for the generation of $SO_4^{\cdot -}$ radicals dates back to 2012 [6]. This work showed that a GO derivative was able to degrade phenol, 2,4-dichlorophenol and methylene blue more efficiently than other carbon catalysts (activated carbon, graphite and carbon nanotubes) and a cobalt-enriched catalyst, due to the presence of structural defects, which can act as active sites. Moreover, nitrogen (N) doping of graphene materials is known to improve the catalytic performance, disrupting the sp^2-hybridized carbon arrangement and modulating the physical, chemical, and electrical properties of the material, creating new active sites [5]. Accordingly, chemically modified or doped graphene derivatives are good catalysts due to their high electrical conductivity, large specific surface area, and efficient electron transfer rate in redox reactions, owing to the high-density sp^2 electrons [1]. Liu *et al.* [9] reported a successful metal-free N-rGO membrane to activate PS for the degradation of phenol. N-rGO was prepared by the hydrothermal method, using ammonia and a commercially available GO material, and the respective membrane was produced by vacuum filtration. The application of catalytic membranes for water treatment is clearly advantageous over conventional powdered materials, as it eliminates the additional procedure of catalyst removal after treatment, being more cost effective and less labour intensive.

So far, the potential of non-metallic GO based catalytic membranes for PS activation has not been fully exploited, since to the best of our knowledge only the study referred above was reported [9]. Therefore, in the present work, graphite oxide was prepared by the modified Hummers' method and different precursors (melamine, urea and gaseous ammonia) were investigated to obtain different N-doped GO samples and to select the most active catalytic material. This strategy allowed to develop for the first time, from the nano- to the macro-scale, an innovative N-doped GO membrane prepared from the modified Hummers' method and applied in PS activation for the degradation of a model industrial pollutant (phenol, Ph) and a low molecular weight carboxylic acid (oxalic acid, OA) commonly found as refractory by-product resulting from the oxidation of many organic pollutants [10].

2. Experimental

2.1. Chemicals

All chemicals were obtained from Sigma-Aldrich, except ethanol that was obtained from Panreac, potassium permanganate from Merck, methanol (HPLC grade) from Fisher chemical and urea from Acros organics. All solutions were prepared with ultrapure water.

2.2. N-doped Graphene oxide fabrication in powder form

Graphite oxide, prepared by the modified Hummers' method [11], was the starting material in this work, and it was produced as described elsewhere [10]. The GO derivatives doped with nitrogen were fabricated and named as described in Table 1. All the synthesised materials were washed with ethanol and water and dried in an oven at 60 °C. For comparison purposes, some characterization data are shown for the GO material (GO-H), which is obtained by drying (ca. 60 °C) the exfoliated (ultrasonic processor UP400S, 24 kHz) graphite oxide aqueous suspension (i.e., this material was not subjected to a temperature of 350 °C).

2.3. Membrane fabrication

Membrane fabrication requires the dispersion of the carbon material in a solvent and, according to a previous publication [14], N-methyl-2-pyrrolidone (NMP) gives the highest solubility value for GO (8.7 μg mL^{-1}) and rGO (9.4 μg mL^{-1}) materials. Hence, NMP was used to disperse the GO derivatives to a concentration of 0.5 g L^{-1}, which were sonicated for 60 min. The dispersion was vacuum filtered onto a Millipore JMWP PTFE substrate, providing a final catalyst mass of 15 mg. The membranes were washed with ethanol and water prior to use.

2.4. Materials characterization

A Quantachrome NOVA 4200e apparatus was used for the textural characterization of the carbon materials by N_2 adsorption at −196 °C, all samples being outgassed for 3 h at 120 °C preceding the analysis. The apparent surface area (S_{BET}) was determined by the Brunauer–Emmett–Teller (BET) equation.

Carbon, hydrogen, nitrogen and sulphur weight percentages were assessed in an elemental analyser from Elementar (Rapid Micro Cube module), whereas the oxygen content was determined by difference.

A Quanta 400 FEG ESEM / EDAX Genesis X4M electron microscope with X-Ray microanalysis and electron backscattered diffraction analysis was used to perform scanning electron microscopy (SEM) analysis.

The attenuated total reflection Fourier transformed infrared (FTIR-ATR) spectra of the GO derivatives were obtained in a JASCO spectrometer (FT/IR-6800), equipped with a ZeSn ATR crystal.

X-ray diffraction (XRD) patterns of the carbon materials were acquired in a PANalytical X'Pert MPD equipment with a X'Celerator detector and secondary monochromator (Cu Kα λ = 0.154 nm, 40 kV, 30 mA; the data were recorded at a 0.017° step size, 100 s/step).

A Kratos AXIS Ultra HSA spectrometer, with a monochromatic Al Kα X-ray source and working at 15 kV (90 W), was employed for X-ray photoelectron spectroscopy (XPS) analysis. Binding energy values were referred to the C1s peak at 285 eV. CasaXPS software was used to analyse and deconvolute the obtained spectra.

High resolution transmission electron microscopy (HRTEM) and scanning transmission electron microscopy (STEM) analysis was performed with a Cs probe-corrected TEM/STEM Jeol ARM 200 CF microscope with a cold-FEG electron source, operated at 80 kV. Jeol Centurio 100 mm^2 Energy dispersive X-ray spectrometer (EDXS) and Gatan Quantum ER Double Electron Energy Loss Spectroscopy (EELS) system were used for elemental analyses and mapping in scanning-transmission mode (STEM). Samples were dispersed in ethanol and placed on a copper lacy-carbon coated grid.

Cross-section specimen preparation and analysis of the membrane was performed with FEI Helios Nanolab 650 dual-beam system (FIB - focused ion beam) using 30 keV Ga ions for cutting and polishing. For chemical analysis and elemental mapping, a MAX 80 silicon drifted detector and an EDXS system from Oxford Instruments were used.

2.5. Catalytic experiments

Catalyst screening experiments with the powdered samples were carried out using 7 mL of 50 mg L^{-1} phenol solution with 1 mM of $Na_2S_2O_8$ and 1gL^{-1} of catalyst load, under stirring in batch mode at room temperature (25 °C). The metal-free carbon membrane was tested in dead-end filtration mode (effective area $A = 0.8 \times 10^{-4}$ m^2) by performing a set of experiments with complete recirculation of the filtrate (Fig. 1 – configuration A) and another set of experiments using continuous flow without recirculation (Fig. 1 – configuration B). In the first set of experiments, 15 mL of a 50 mg L^{-1} phenol solution (pH 6.6–7.0), or a 90 mg L^{-1} oxalic acid solution (natural pH 3.0), containing 1 mM of PS, was recirculated through the membrane at a flow rate of 1.5 mL min^{-1} (provided by a peristaltic pump) and room temperature (25 °C). Similar conditions were tested in the second set of experiments, but in this case the filtrate was not recirculated as feed and the initial phenol concentration was 5 mg L^{-1}. Prior to PS activation by the metal-free carbon membrane, adsorption of the tested pollutants onto the membrane was evaluated. The pollutant concentration was analysed immediately after sampling.

2.6. Analytical techniques

The phenol concentration was analysed by high performance liquid chromatography (HPLC) with a Hitachi Elite LaChrom apparatus equipped with a diode array detector (L-2450, at 270 nm) and a Lichrocart Purospher Star RP-18 endcapped column (250 mm × 4.6 mm, 5 µm particles), with a mobile phase of water: methanol (70:30) in a gradient step, at a fixed flow rate of 1 mL min^{-1} and at room temperature [15,16]. The oxalic acid concentration was also determined by HPLC, but in this case with an UV detector (at 200 nm) and an Alltech OA-1000 column (300 mm × 6.5 mm; 9 µm particles) under isocratic elution with 5 mM of H_2SO_4, at 0.5 mL min^{-1} and at room temperature [10]. The total organic carbon (TOC) content was monitored in a Shimadzu TOC-L equipment.

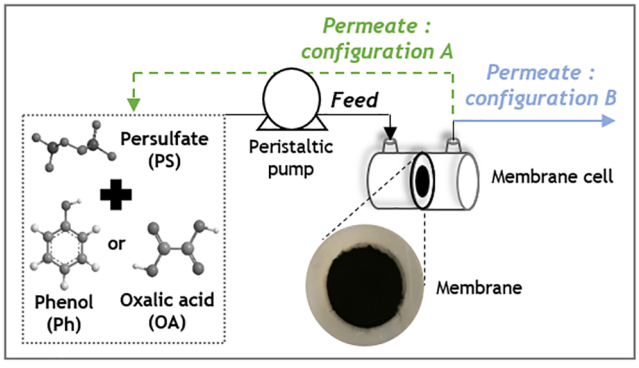

Fig. 1. Schematic representation of the experimental set-up to test the membrane (rGO-M (0.4)) under recirculation (configuration A) and continuous mode (configuration B).

3. Results and discussion

3.1. Materials characterization

The results from elemental analysis and nitrogen adsorption-desorption isotherms are shown in Table 2. The highest nitrogen percentage (23.78 wt%) was obtained for the GO material doped with melamine (rGO-M (0.4)). The small nitrogen content present in rGO (1.35 wt%) results from $NaNO_3$, which is employed for graphite oxidation in the modified Hummers' method, small percentages of nitrogen being reported in the literature even for commercial graphene flakes [17]. All the materials had a small specific surface area (5–25 m^2 g^{-1}), due to the stretched assembly of the GO sheets when the suspension is dried to obtain the nitrogen adsorption–desorption isotherms, including those samples prepared with different amounts (0.2, 0.8 and 1.6 g) of melamine (6–8 m^2 g^{-1}). rGO-A is the material with the highest surface area probably due to the more extensive thermal treatment that was performed for this material.

Specific functional groups of the fabricated materials were observed by FTIR-ATR (Fig. 2). The FTIR-ATR spectrum of rGO-M (0.4) showed

Table 2
Elemental analysis of the carbon materials and specific surface area (S_{BET}).

Sample	S_{BET} (m^2 g^{-1})	N [wt%]	C [wt%]	H [wt%]	S wt%]	O [wt%]
rGO	6	1.35	76.09	1.13	0.27	21.17
rGO-A	25	11.19	76.52	1.05	0.23	11.01
rGO-U	5	13.27	70.77	1.24	0.80	13.92
rGO-M (0.4)	8	23.78	57.96	1.86	1.29	15.11
Used rGO-M (0.4) membrane material	n.d.	21.68	60.27	1.92	0.65	15.48

n.d. – not determined

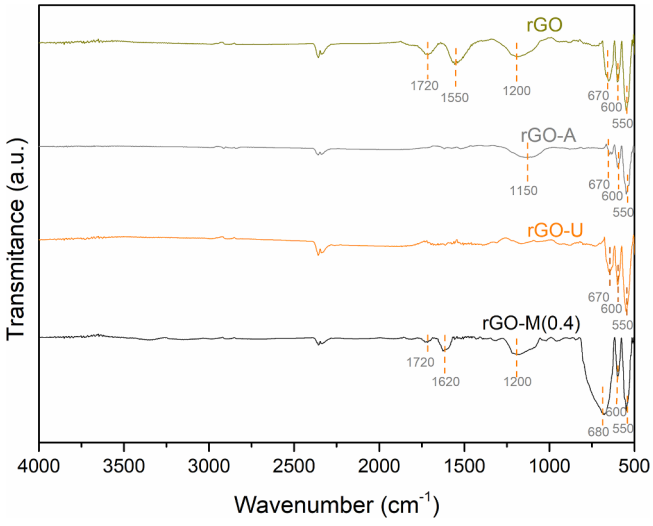

Fig. 2. FTIR-ATR spectra of the GO-derivatives.

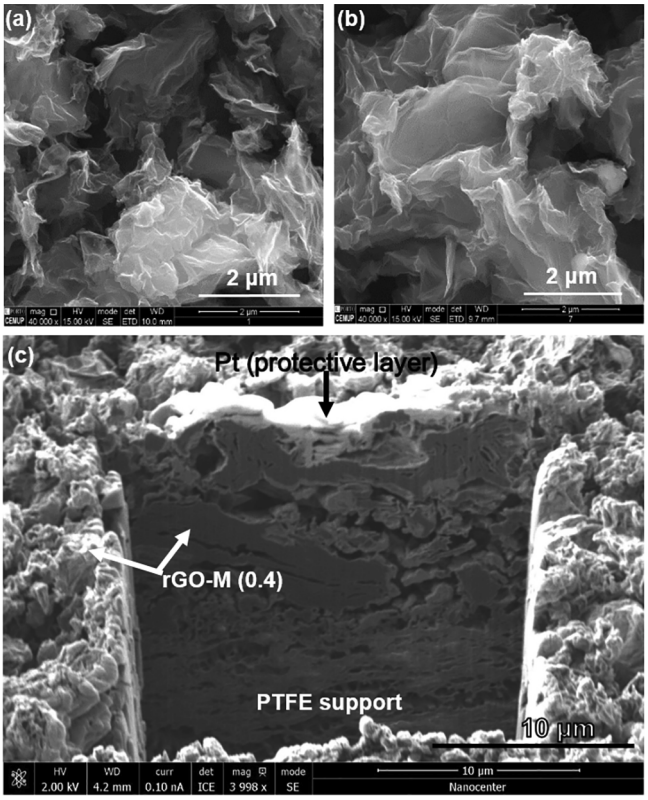

Fig. 3. SEM micrographs of rGO-M (0.4) (a), rGO (b) and rGO-M (0.4) membrane FIB cross-section (c) - Pt corresponds to the protective layer used for analysis.

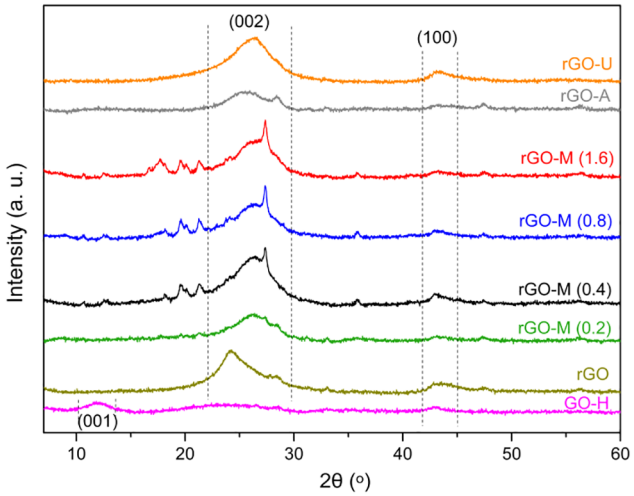

Fig. 4. XRD patterns of studied samples.

the occurrence of a band at ca. 1620 cm^{-1}, corresponding to the N—H bending of primary amine groups ($-NH_2$). The rGO-A sample presented a broad band at around 1150 cm^{-1}, indicative of the C—N stretching from a secondary amine. On the other hand, rGO-U did not present any evident typical peak associated to nitrogen functional groups. The rGO sample presented bands at ca. 550, 600, 670, 1200, 1550 and 1720 cm^{-1}, which can be attributed to —OH out of plane bending, C—H bending, C=C bending, C—OH stretching, sp^2 aromatic C=C bonds and carbonyl groups (C=O), respectively. Some of these bands can be seen in other samples.

The material with highest nitrogen content (also presenting the highest catalytic activity for the degradation of phenol, as demonstrated below), i.e. rGO-M (0.4), as well as undoped rGO and/or GO-H, were additionally characterized by SEM (Fig. 3), XRD (Fig. 4), HRTEM (Figs. 5 and 6) and XPS (Fig. 7).

From the SEM micrographs (Fig. 3), it can be inferred that the GO treatment with melamine (rGO-M (0.4)) did not alter the typical sheet-like appearance of rGO, meaning that N-doping does not destroy the physical morphology of the original carbon material. Furthermore, the cross-section of the rGO-M (0.4) membrane revealed its morphology (Fig. 3c).

The XRD patterns of the GO precursor (GO-H) and all other samples are shown in Fig. 4. GO-H presented a (0 0 1) diffraction peak at ca. 2θ = 11.95°, indicative of an interlayer distance (d-distance) of 0.74 nm, as calculated with the Bragg's equation. This peak disappeared and a (0 0 2) diffraction peak appeared for the reduced samples, specifically at 2θ = 26.02° for rGO-M (0.4), which corresponds to a d-distance of 0.34 nm. Thus, the d-distance was smaller for rGO-M (0.4) comparatively to GO-H, as expected since the distance between layers is commonly attributed to the oxygen surface groups (such as epoxy, hydroxyl, carboxyl and carbonyl groups) abundant in the non-reduced material [18]. The (1 0 0) diffraction peak was found around 2θ = 42.5°. The Scherrer's equation (constant of 0.9) was applied to the (1 0 0) and (0 0 2) diffraction peaks of rGO-M (0.4), and to (1 0 0) and (0 0 1) in the case of GO-H, the determined average crystallite size being 1.9 and 4.1 nm, respectively. Regarding the patterns of rGO-M (0.2), rGO-M (0.8), rGO-M (1.6), rGO-A and rGO-U, both (0 0 2) and (1 0 0) diffraction peaks are observed, small peaks between 17.5° and 21.5° appearing as higher is the amount of melamine employed in the preparation of rGO-M samples.

The results obtained by HRTEM characterization of GO-H, including both high-angle annular dark-field (HAADF-STEM) and bright-field (BF-STEM) modes, are shown in Fig. 5. Aggregated GO flakes are clearly observed in Fig. 5a-c, with sizes up to 50 nm. Those flakes are mostly perpendicular to the electron beam (in [00.1] orientation regarding to the beam), still some of them are curved so that part of the flakes are parallel to the beam (⟨10.1⟩ types of orientations). The bright spots in atomically resolved HAADF-STEM micrograph (Fig. 5d) where the intensity strongly depends on atomic number (Fig. 5b and d) correspond to the oxygen atoms, concentrated at the edge of GO flakes which are curved so that we can estimate its thickness. From low-loss EELS spectra where the maximum of σ + π plasmon was around 24 eV (not shown), it is concluded that GO flakes in average consist of at least 10 sheets [19]. The core-loss EELS spectrum from thin area (Fig. 5f) displays a very low concentration of O atoms.

Regarding the rGO-M (0.4) sample, some heterogeneity was observed (Fig. 6). For instance, in Fig. 6a is shown the rGO structure obscured with an amorphous layer, the EELS spectrum (Fig. 6c) revealing the presence of both nitrogen and oxygen in this zone. However, some other flakes of the same sample have zones without or with low concentration of nitrogen and oxygen at the edges (Fig. 6b and d). The EELS spectrum of an area with visible crystalline structure, but without noticeable amounts of O and N (Fig. 6d), shows a characteristic sharp line (peak) in C K edge (in σ* part), while in the amorphous area with high O and N contents, this line is hardly seen or even missing.

HRTEM, HRTSTEM and EELS results are in good agreement with XRD results, since the d-distance obtained with XRD and SAED (selected area electron diffraction) can be directly compared. In Fig. S1 there is an electron diffraction pattern of GO-H from an area with three layers of GO rotated within angle of 7.4° – the zone axis is [0 0 0 1] (perpendicular to basal planes). Measured d-distance values for the 10 plane from SAED diffraction pattern (0.21 nm) are in good agreement with measured values for lines (1 0 0) from XRD pattern (0.21 nm).

The information about sheet thickness can be directly obtained from HRTEM (or HRSTEM) images, which is around ~3 nm in the case of GO-H, i.e. in good agreement with ~4 nm obtained from XRD. In the case of rGO-M (0.4), the thickness of the crystalline part of the flakes

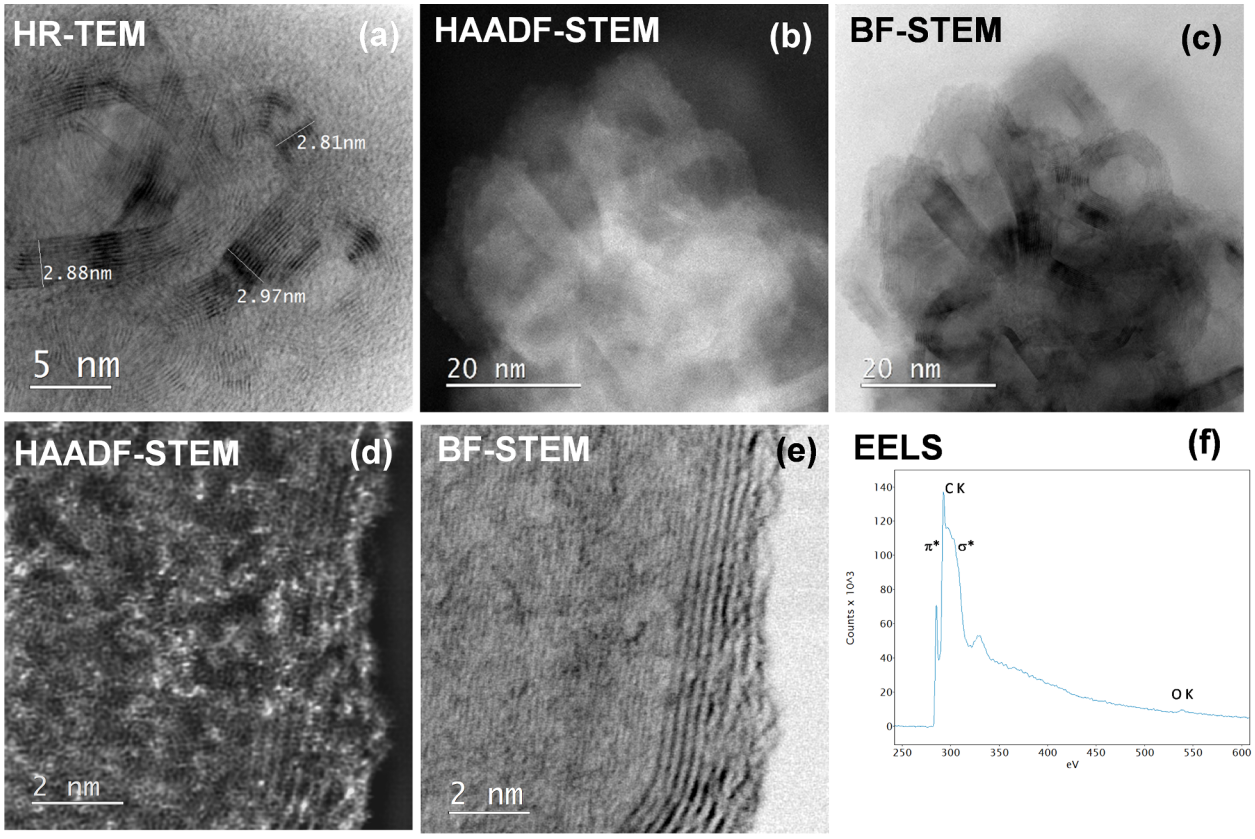

Fig. 5. HRTEM micrograph (a), HAADF-STEM (b, d), BF-STEM (c, e) and EELS spectrum (f) of GO-H.

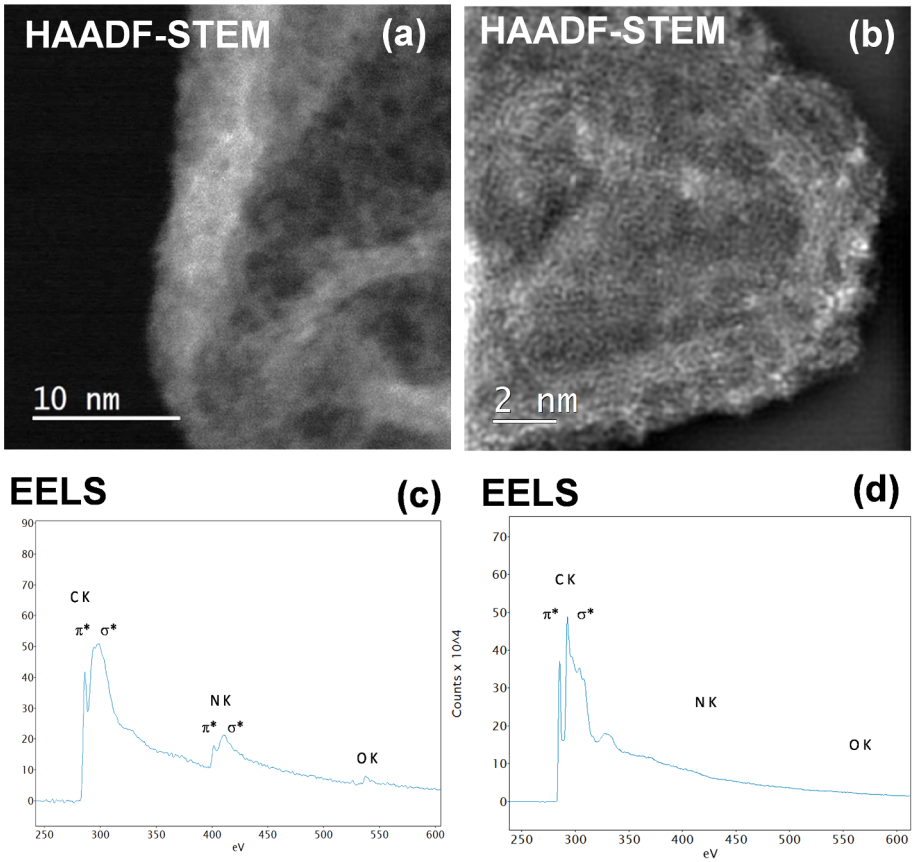

Fig. 6. HAADF-STEM of rGO-M (0.4): amorphous zone with high amount of nitrogen (a), crystalline zone without O and N (b), and EELS spectra (c and d, respectively). Note the difference in the σ* line structure indicating the amorphous and crystalline nature of the investigated areas.

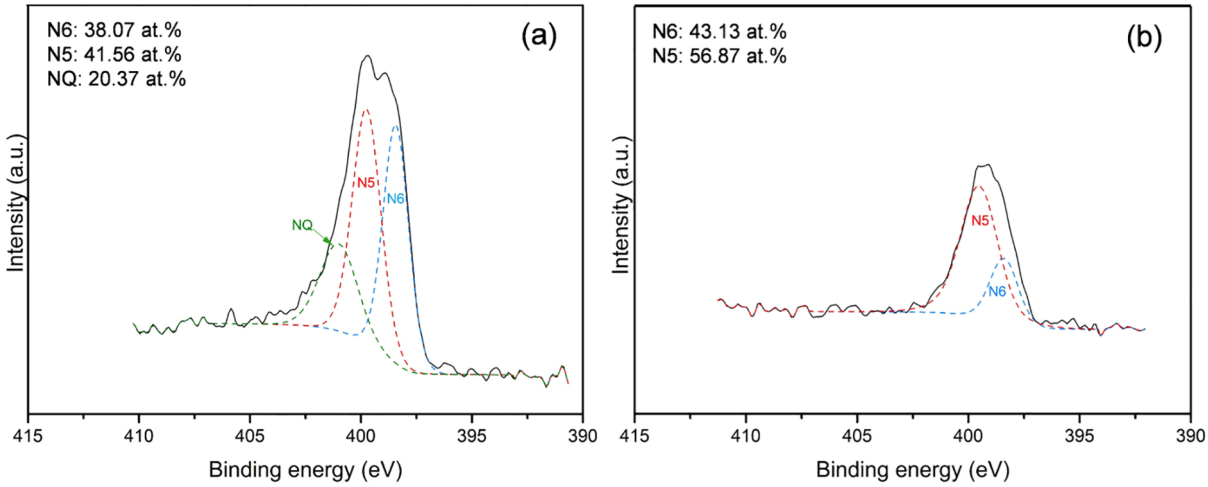

Fig. 7. Deconvoluted N1s spectra of rGO-M (0.4) (a) and rGO (b), N5, N6 and NQ corresponding to N-pyrrolic, N-pyridinic and N-quaternary species.

was measured in reciprocal space, being around 2 nm, which is comparable to the XRD value (1.9 nm). XPS analysis of the N1s region was performed to further understand the nature of the N-functionalities in rGO and rGO-M (0.4) samples (Fig. 7). The rGO-M (0.4) sample (Fig. 7a) presented 41.56, 38.07 and 20.37 at.% of N-pyrrolic (N5), N-pyridinic (N6) and N-quaternary (NQ) species, respectively, while the rGO sample (Fig. 7b) had some N5 (56.87 at.%) and N6 (43.13 at.%) species. In the literature, the use of N-doped graphene powdered materials for PMS or PS activation has been reported for phenol degradation, i.e. Li et al. [13] prepared similar N-doped graphene derivatives using melamine, and the XPS analysis revealed 48.70, 39.50 and 11.80 at.% of N6, N5 and NQ species, respectively. Similarly, Duan *et al.* [5] reported a melamine-doped GO material, treated at 700 °C, with 54.42, 23.09 and 22.49 at.% of N6, N5 and NQ. The percentage of nitrogen species in these works presents some differences (N6 > N5 > NQ) in comparison to the rGO-M (0.4) sample of the present study (N5 > N6 > NQ). Nevertheless, the higher abundance of N5 in comparison with N6 has been reported for other N-doped GO materials [9]. Regarding the materials prepared with different amounts of melamine, a higher percentage of NQ and N6 was determined in rGO-M (0.4) (Fig. 7a) than in samples prepared with higher amounts of melamine (Fig. S2).

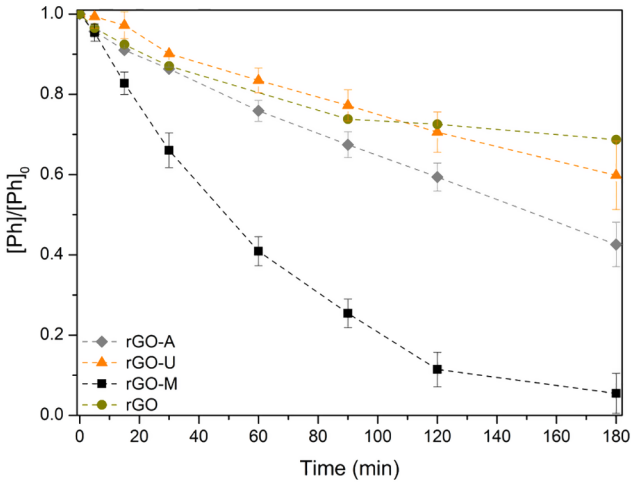

Fig. 8. Phenol (Ph) degradation by PS activation with different powdered carbon catalysts. Experimental conditions: 7 mL of [Ph] = 50 mg L^{-1}; [PS] = 1 mM; $pH_{initial}$: 6.6–7.0; Catalyst load = 1gL^{-1}; under stirring and at 25 °C.

3.2. Catalytic performance

It has been documented that phenol oxidation by PS activation alone cannot occur [2,9]. Therefore, a catalyst is needed to activate PS in order to degrade the aromatic compound. An initial screening of the catalytic activity of the fabricated N-doped powders for the removal of phenol was performed in batch mode (Fig. 8).

Among the tested catalysts, the N-doped GO powder prepared with melamine (rGO-M (0.4)) presented the highest phenol removal (i.e. 96% after 180 min). This outcome clearly confirms that the nitrogen precursor used for the functionalization of GO plays an important role in the properties and catalytic performance of the material. Li *et al.* [13] have found urea as the best nitrogen precursor for the synthesis of N-doped graphene catalysts, since it outperformed catalysts prepared with other precursors (like melamine, ammonium nitrate and cyanamide) in the PMS activation for phenol degradation. In the present study, the rGO-M (0.4) catalyst with the highest nitrogen percentage (23.78 wt%) provided the highest removal of phenol. Thus, different amounts of melamine (0.2, 0.4, 0.8 and 1.6 g) were tested in order to evaluate its effect on the catalytic activity of the N-doped GO material (Fig. 9). The synthesis conducted with 0.4 g of melamine revealed the highest phenol degradation. These findings are in line with the XPS analysis of the N1s

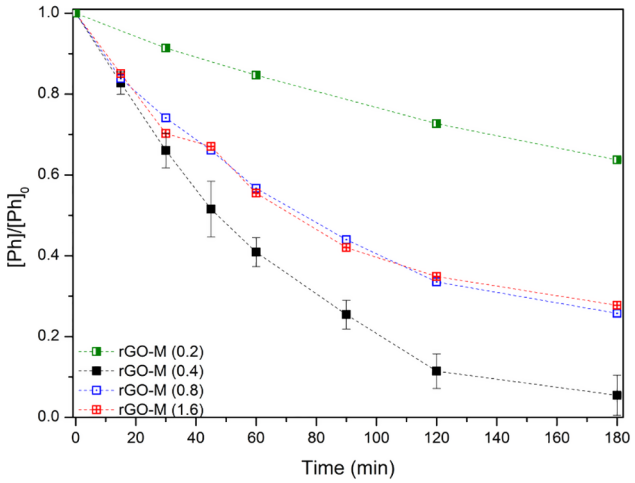

Fig. 9. Phenol (Ph) degradation by PS activation with GO catalysts doped with different amounts of melamine (0.2, 0.4, 0.8 and 1.6 g). Experimental conditions: 7 mL of [Ph] = 50 mg L^{-1}; [PS] = 1 mM; $pH_{initial}$: 6.6–7.0; Catalyst load = 1gL^{-1}; under agitation and at 25 °C.

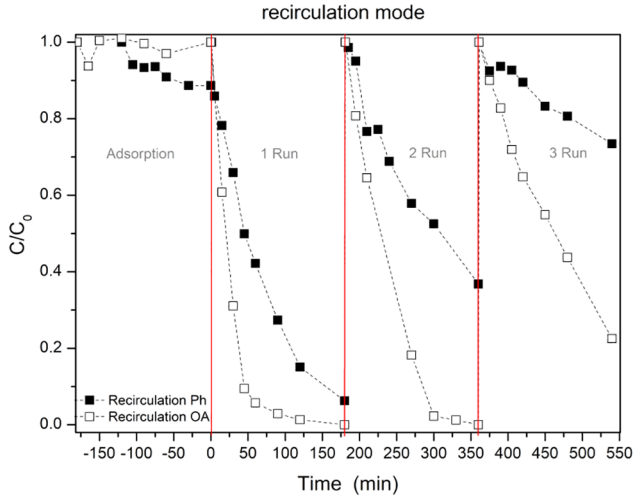

Fig. 10. Reusability assessment of rGO-M (0.4) catalytic membranes for the degradation of phenol (Ph) and oxalic acid (OA) by PS activation. Experimental conditions: 15 mL of $[Ph]_{initial}$ = 50 mg L^{-1} or $[OA]_{initial}$ = 90 mg L^{-1}; [PS] = 1 mM; $pH_{initial}$ of Ph = 6.6–7.0 and $pH_{initial}$ of OA = 3.0 (natural pH); 1.5 mL min^{-1}; under recirculation mode and at 25 °C.

region of the samples prepared with melamine (Fig. 7a and Fig. S2), which revealed a higher percentage of NQ and N6 species in rGO-M (0.4) than in materials prepared with higher amounts of melamine. NQ species were referred in the literature as those contributing to a higher catalytic activity in the PS activation reaction [5]. It has been also reported the reduction of N6 species for a sample doped with urea that was used in one cycle of phenol degradation by PMS activation [13], thus evidencing the importance of N6 species in this type of reaction, besides the NQ groups.

Given that rGO-M (0.4) was the most active catalyst for the degradation of phenol by PS activation, it was used to produce membranes. The fabricated rGO-M (0.4) membranes were subsequently tested, under recirculation mode, for the PS activation in the degradation of phenol and oxalic acid, for 3 consecutive runs with the same membrane (Fig. 10). Prior to the catalytic reactions, adsorption experiments (without PS addition) were carried out with 50 mg L^{-1} of phenol and 90 mg L^{-1} of oxalic acid, showing negligible removal by adsorption of either pollutant on the membrane (Fig. 10). However, the removal of oxalic acid by PS activation was 100% in the first recirculation run after 180 min (i.e., its concentration decreased to values below the limit of quantification) and kept for the second cycle after the same period of time, decreasing in the third one. Regarding the catalytic oxidation of phenol, 94% of its removal was achieved in the first cycle, but the performance decreased to 63 and 27% of degradation after 180 min in the second and third runs, respectively. The TOC values followed the same tendency as the phenol removal cycles, namely 55% of mineralization after the first run, a value that was gradually reduced to 35 and 8% after the second and third cycles, respectively. Results were not found in the literature for the oxalic acid degradation by PS activation. However, the lower catalytic activity after the first run has been observed previously with N-doped GO and rGO catalysts in the powdered form for phenol oxidation by PMS activation. The lower catalytic activity has been attributed to the adsorption of reaction by-products and pollutant molecules onto the reaction sites of the carbon material, thus compromising its catalytic activity for further reuses [5,20,21]. Furthermore, a recent study [22] reported a GO erosion after PS activation, due to radical attack on GO, leading to the formation of GO fragments.

The significance of the pH in this type of catalytic reaction has been reported, the initial pH between 6.5 and 7.0 being considered the ideal for the oxidation of phenolic compounds [13]. The pH was monitored after every reaction cycle with phenol, and again the trend was identical, with a sharp decrease after first run (pH 2.7) that was kept almost constant for the second (pH 2.9) and third (pH 3.2) runs, most probably due to the formation of low-molecular weight carboxylic acids. In the case of oxalic acid, the pH after each run was very similar to the initial and natural pH of the oxalic acid solution (pH ~ 3.0) contrarily to what was observed in the degradation of phenol, where the values decreased significantly after the first run.

To better investigate the reasons behind the lower catalytic activity of the rGO-M (0.4) membrane after use, the material recovered from the membrane was characterized. SEM imaging (Fig. 11a) showed a morphology similar to the fresh one (Fig. 3a). However, elemental analysis (Table 2) revealed a lower percentage of nitrogen in the used membrane material (21.68 wt%) relatively to the pristine one (23.78 wt%), the deviation of triplicates being ± 0.15 wt% and 0.01 wt%, respectively. Thus, this difference of ca. 2 wt% can be ascribed to the loss of nitrogen functionalities throughout the catalytic reaction [23]. Nevertheless, the FTIR-ATR spectrum of the used membrane material (Fig. S3) showed similarities to the pristine one (Fig. 2). Moreover, XPS analysis of the membrane material performed after one cycle (Fig. 11b) showed the absence of N6 groups. This result can explain the decreased catalytic activity with each cycle, since it has been shown that N6 species have a pair of lone electrons, which can change the valance

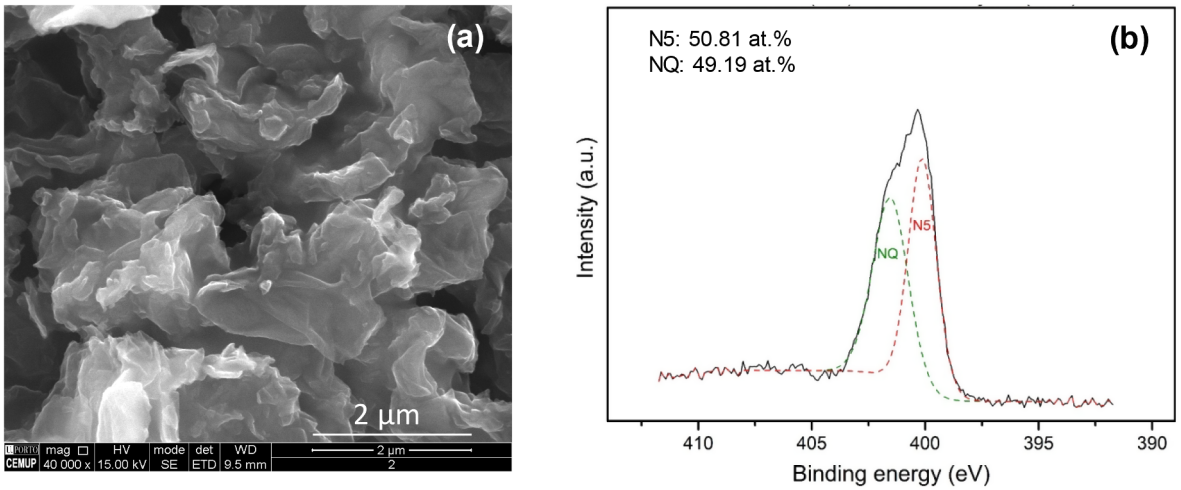

Fig. 11. SEM image of the rGO-M (0.4) membrane material used for PS activation in phenol degradation (a) and its deconvoluted N1s spectrum, showing only the presence of pyrrolic (N5) and quaternary (NQ) nitrogen species (b).

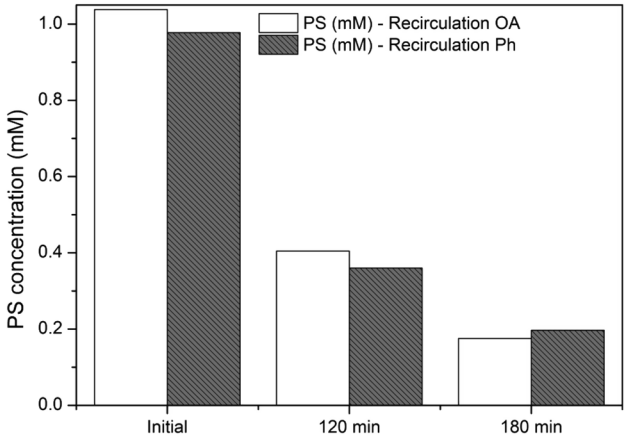

Fig. 12. Persulfate concentration along the experiments with the rGO-M (0.4) membrane under recirculation mode.

band of graphene-based materials and enhance the π states of Fermi level [24]. Additionally, as referred above, the reduction of the N6 species has been reported in the literature for a sample doped with urea that was used for phenol degradation by PMS activation (from 100% of phenol removal in the 1st run to 83.1% in the 3rd run) [13], thus evidencing the importance of N6 species in this type of reaction. Furthermore, the nitrogen-rich active sites can be obstructed by the accumulation of PS and/or by-products on the membrane, which could also compromise its reusability. These findings attested the importance of the composition of the carbocatalysts, which extensively impacted their redox potential, influencing electron transfer from the carbon material to PS or PMS [2]. However, Fig. 11b also shows that NQ species were not lost, in contrast with N6, suggesting that even if some decrease of the catalytic activity is expected, NQ could contribute to maintain some of the material catalytic activity.

The PS concentration was also determined in both phenol and oxalic acid degradation experiments (Fig. 12), following the methodology described elsewhere [25]. As expected, the PS concentration decreased throughout each experiment, in both cases reaching ca. 0.20 mM of PS after 180 min. Thus, ca. 80% of PS is consumed in 180 min, 100% and 94% of oxalic acid and phenol degradation, respectively, being achieved at this reaction time.

Regarding the reactive oxygen species (ROS) involved in this reaction, three pathways for PS and PMS activation were recently summarized for carbon materials [4]. The first relies on the generation of $SO_4^{\cdot -}$ and $HO^{\cdot}$ radicals; the second corresponds to a non-radical mechanism that can include the formation of singlet oxygen ($^1O_2$), the development of a charge transfer complex and/or direct catalysis; and the third is a combination of radical and non-radical pathways. In the present work, the active radicals involved in the reaction were studied using both phenol (Fig. 13a) and oxalic acid (Fig. 13b). Methanol (MeOH) was employed as scavenger of $SO_4^{\cdot -}$ and $HO^{\cdot}$ radicals and furfuryl alcohol (FFA) as scavenger of $^1O_2$, in a molar ratio of 1000:1 (scavenger: PS) [26]. The phenol degradation by PS activation with the rGO-M (0.4) membrane and the tested scavengers (Fig. 13a) suggests that $^1O_2$ is the main ROS involved in this catalytic reaction: the removal of phenol was only 10% after 180 min in the presence of FFA, whereas removals of 88% and 94% were respectively obtained with MeOH and without scavengers after the same period of time. The significant contribution of $^1O_2$ in this reaction was confirmed when oxalic acid was employed as probe molecule (Fig. 13b), the degradation of this organic compound decreasing to 59% after 180 min in the presence of FFA, comparatively to 100% removal without scavengers and 93% in the presence of MeOH. Thus, the catalytic mechanism is governed by both the radical and the non-radical pathways, but a more notorious contribution was observed from the non-radical one ($^1O_2$). The high reactivity of $^1O_2$ has been described in the literature, in particular towards electron-rich molecules like phenol [2,27], some studies also reporting the occurrence of the non-radical pathway for PMS activation with N-doped graphene derivatives [13,28–31].

The rGO-M (0.4) membrane was also tested under continuous filtration for the degradation of phenol and oxalic acid without recirculation of the filtrate (Fig. 14). Interestingly, a high removal of phenol was observed by PS activation with the rGO-M (0.4) membrane at the beginning of the experiment, decreasing significantly after 30 min, but achieving a stable removal of phenol (ca. 30%) in continuous mode after 4 h, with a mineralization of 10.2% and the filtrate having pH 3.6. Once again, N6 species were not detected by XPS analysis of the membrane used in this experiment, while NQ and N5 species remain in the used membrane (not shown). Moreover, the oxalic acid removal was nearly 25% and quite stable during the experiment, as well as the respective pH, when the experiment was performed with the highest concentration of this pollutant (90 mg L^{-1}). The oxalic acid removal significantly increased up to 65% in 3 h (and was maintained after this period of time) when its initial concentration was decreased (to 30 mg L^{-1}). Considering that these experiments were performed with quite high concentrations, these results demonstrate that this metal-free catalytic membrane is highly active, its performance

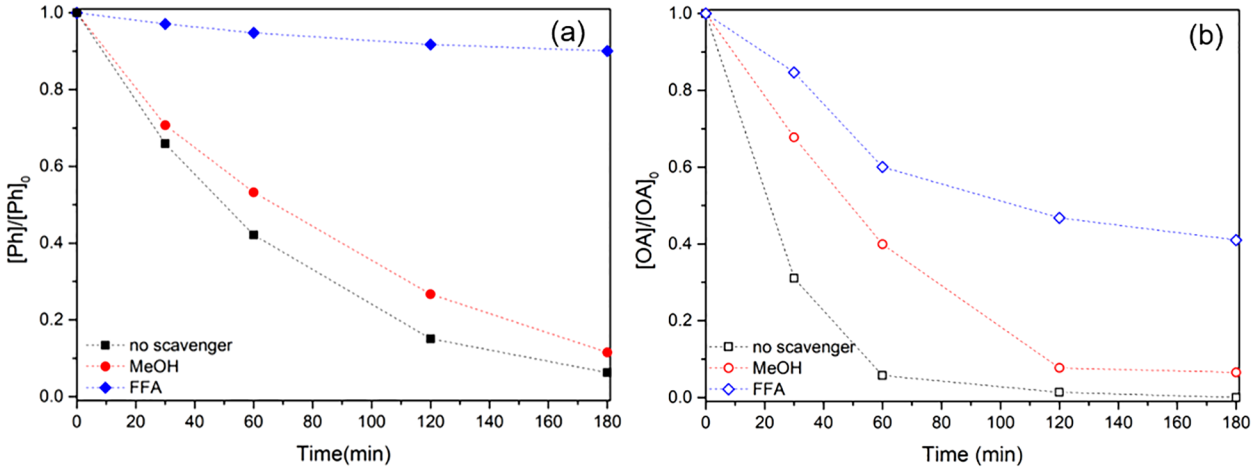

Fig. 13. Phenol (Ph) (a) and oxalic acid (OA) (a) degradation by persulfate activation with rGO-M (0.4) catalytic membranes and scavengers (methanol, MeOH and furfuryl alcohol, FFA). Preliminary adsorption tests are performed without PS. Experimental conditions: $[Ph]_{initial}$ = 50 mg L^{-1} or $[OA]_{initial}$ = 90 mg L^{-1}; [PS] = 1 mM; [scavenger] = 1000 mM; $pH_{initial}$ of Ph = 6.6–7.0 and $pH_{initial}$ of OA = 3.0 (natural pH); 1.5 mL min^{-1}; under recirculation mode and 25 °C.

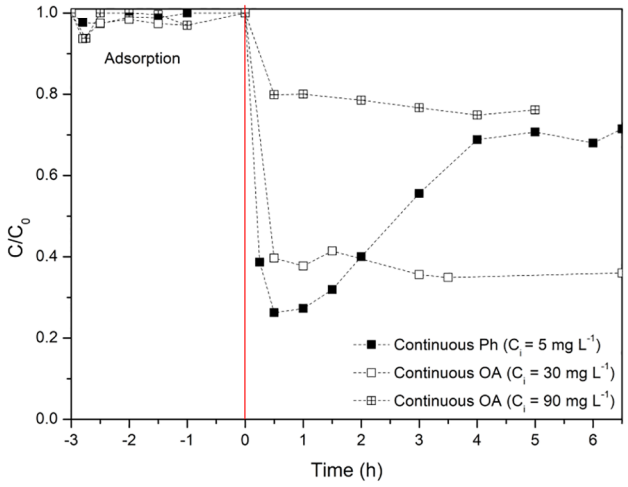

Fig. 14. Phenol (Ph - $[Ph]_{initial} = 5\,mg\ L^{-1}$) and oxalic acid (OA – $[OA]_{initial} = 30$ and $90\,mg\ L^{-1}$) degradation by persulfate activation with rGO-M (0.4) catalytic membranes. Preliminary adsorption tests are performed without PS. Experimental conditions: [PS] = 1 mM; $pH_{initial}$ of Ph = 6.6–7.0 and $pH_{initial}$ of OA = 3.0 (natural pH); $1.5\,mL\,min^{-1}$; under continuous mode and at 25 °C.

depending on the initial pollutant concentration or, as alternative, the water flow rate. Thus, these results demonstrate the potentialities of this type of metal-free catalytic membranes for water treatment in continuous mode, but more studies are needed, for instance performing experiments with realistic matrices where the pollutants are often at much lower concentrations, better performances being expected. The findings suggest that both N6 and NQ species play a positive role in the catalytic activity of this membrane, but N6 species are lost when the material is used, in contrast with NQ species.

4. Conclusions

A N-doped GO powdered material with high catalytic activity for persulfate activation and phenol degradation was prepared using melamine as precursor. The respective membrane lost some of its catalytic activity during filtration, due to the loss of N-pyridinic groups, in contrast with the N-quaternary species that were detected in the used membrane. In fact, after a certain period of time in continuous mode, the catalytic activity is kept constant under a constant feed of the organic pollutants. Singlet oxygen reactive species were determined as the main responsible for the degradation of the target pollutants. Thus, the present study demonstrates the potentialities of this type of metal-free immobilized catalysts, cutting back on expenses and labor associated with catalyst separation from treated water. However, further research is needed regarding the optimization of the operating conditions and the performance with realistic matrices.

Acknowledgments

This work was financially supported by project NORTE-01-0145-FEDER-031049 (InSpeCt) funded by FEDER funds through NORTE 2020 - Programa Operacional Regional do NORTE and by national funds (PIDDAC) through FCT/MCTES. We would also like to thank the scientific collaboration under project "AIProcMat@N2020 – Advanced Industrial Processes and Materials for a Sustainable Northern Region of Portugal 2020" (NORTE-01-0145-FEDER-000006; NORTE 2020 - Portugal 2020 Partnership Agreement, through FEDER) and project "POCI-01-0145-FEDER-006984 – Associate Laboratory LSRE-LCM" (FEDER through COMPETE2020 - Programa Operacional Competitividade e Internacionalização (POCI) and FCT). MP and GD acknowledge the PhD research grant from FCT (SFRH/BD/102086/2014) and the Slovenian Research Agency (P2-0393), respectively. Technical assistance with SEM and XPS analysis is gratefully acknowledged to CEMUP team and Dr. Carlos Sá.

Appendix A. Supplementary data

Supplementary data to this article can be found online at https://doi.org/10.1016/j.cej.2019.02.211.

References

[1] Q. Zhao, Q. Mao, Y. Zhou, J. Wei, X. Liu, J. Yang, L. Luo, J. Zhang, H. Chen, H. Chen, L. Tang, Metal-free carbon materials-catalyzed sulfate radical-based advanced oxidation processes: a review on heterogeneous catalysts and applications, Chemosphere 189 (2017) 224–238.
[2] J. Wang, S. Wang, Activation of persulfate (PS) and peroxymonosulfate (PMS) and application for the degradation of emerging contaminants, Chem. Eng. J. 334 (2018) 1502–1517.
[3] C. Zhu, F. Zhu, D.D. Dionysiou, D. Zhou, G. Fang, J. Gao, Contribution of alcohol radicals to contaminant degradation in quenching studies of persulfate activation process, Water Res. 139 (2018) 66–73.
[4] R. Xiao, Z. Luo, Z. Wei, S. Luo, R. Spinney, W. Yang, D.D. Dionysiou, Activation of peroxymonosulfate/persulfate by nanomaterials for sulfate radical-based advanced oxidation technologies, Curr. Opin. Chem. Eng. 19 (2018) 51–58.
[5] X. Duan, Z. Ao, H. Sun, S. Indrawirawan, Y. Wang, J. Kang, F. Liang, Z.H. Zhu, S. Wang, Nitrogen-doped graphene for generation and evolution of reactive radicals by metal-free catalysis, ACS Appl. Mater. Interfaces 7 (2015) 4169–4178.
[6] H. Sun, S. Liu, G. Zhou, H.M. Ang, M.O. Tade, S. Wang, Reduced graphene oxide for catalytic oxidation of aqueous organic pollutants, ACS Appl. Mater. Interfaces 4 (2012) 5466–5471.
[7] P. Sun, H. Liu, Z. Zhai, X. Zhang, Y. Fang, J. Tan, J. Wu, Degradation of UV filter BP-1 with nitrogen-doped industrial graphene as a metal-free catalyst of peroxymonosulfate activation, Chem. Eng. J. 356 (2019) 262–271.
[8] L. Bekris, Z. Frontistis, G. Trakakis, L. Sygellou, C. Galiotis, D. Mantzavinos, Graphene: a new activator of sodium persulfate for the advanced oxidation of parabens in water, Water Res. 126 (2017) 111–121.
[9] Y. Liu, L. Yu, C.N. Ong, J. Xie, Nitrogen-doped graphene nanosheets as reactive water purification membranes, Nano Res. 9 (2016) 1983–1993.
[10] M. Pedrosa, L.M. Pastrana-Martínez, M.F.R. Pereira, J.L. Faria, J.L. Figueiredo, A.M.T. Silva, N/S-doped graphene derivatives and TiO_2 for catalytic ozonation and photocatalysis of water pollutants, Chem. Eng. J. 348 (2018) 888–897.
[11] W.S. Hummers, R.E. Offeman, Preparation of graphitic oxide, J. Am. Chem. Soc. 80 (1958) 1339–1340.
[12] X. Li, H. Wang, J.T. Robinson, H. Sanchez, G. Diankov, H. Dai, Simultaneous nitrogen doping and reduction of graphene oxide, J. Am. Chem. Soc. 131 (2009) 15939–15944.
[13] D. Li, X. Duan, H. Sun, J. Kang, H. Zhang, M.O. Tade, S. Wang, Facile synthesis of nitrogen-doped graphene via low-temperature pyrolysis: The effects of precursors and annealing ambience on metal-free catalytic oxidation, Carbon 115 (2017) 649–658.
[14] D. Konios, M.M. Stylianakis, E. Stratakis, E. Kymakis, Dispersion behaviour of graphene oxide and reduced graphene oxide, J. Colloid Interface Sci. 430 (2014) 108–112.
[15] M.J. Sampaio, R.R. Bacsa, A. Benyounes, R. Axet, P. Serp, C.G. Silva, A.M.T. Silva, J.L. Faria, Synergistic effect between carbon nanomaterials and ZnO for photocatalytic water decontamination, J. Catal. 331 (2015) 172–180.
[16] R.P. Rocha, A.G. Gonçalves, L.M. Pastrana-Martínez, B.C. Bordoni, O.S.G.P. Soares, J.J.M. Orfão, J.L. Faria, J.L. Figueiredo, A.M.T. Silva, M.F.R. Pereira, Nitrogen-doped graphene-based materials for advanced oxidation processes, Catal. Today 249 (2015) 192–198.
[17] M.P. Araújo, O.S.G.P. Soares, A.J.S. Fernandes, M.F.R. Pereira, C. Freire, Tuning the surface chemistry of graphene flakes: new strategies for selective oxidation, RSC Adv. 7 (2017) 14290–14301.
[18] Y. Li, W. Gao, L. Ci, C. Wang, P.M. Ajayan, Catalytic performance of Pt nanoparticles on reduced graphene oxide for methanol electro-oxidation, Carbon 48 (2010) 1124–1130.
[19] A. Politano, G. Chiarello, Plasmon modes in graphene: status and prospect, Nanoscale 6 (2014) 10927–10940.
[20] H. Sun, Y. Wang, S. Liu, L. Ge, L. Wang, Z. Zhu, S. Wang, Facile synthesis of nitrogen doped reduced graphene oxide as a superior metal-free catalyst for oxidation, Chem. Commun. 49 (2013) 9914–9916.
[21] X. Duan, S. Indrawirawan, H. Sun, S. Wang, Effects of nitrogen-, boron-, and phosphorus-doping or codoping on metal-free graphene catalysis, Catal. Today 249 (2015) 184–191.
[22] Z. Wang, L. Sun, X. Lou, F. Yang, M. Feng, J. Liu, Chemical instability of graphene oxide following exposure to highly reactive radicals in advanced oxidation processes, J. Colloid Interface Sci. 507 (2017) 51–58.
[23] J. Kang, X. Duan, L. Zhou, H. Sun, M.O. Tadé, S. Wang, Carbocatalytic activation of persulfate for removal of antibiotics in water solutions, Chem. Eng. J. 288 (2016) 399–405.
[24] Z. Luo, S. Lim, Z. Tian, J. Shang, L. Lai, B. MacDonald, C. Fu, Z. Shen, T. Yu, J. Lin, Pyridinic N doped graphene: synthesis, electronic structure, and electrocatalytic

property, J. Mater. Chem. 21 (2011).
[25] S. Gokulakrishnan, A. Mohammed, H. Prakash, Determination of persulphates using N, N-diethyl-p-phenylenediamine as colorimetric reagent: oxidative coloration and degradation of the reagent without bactericidal effect in water, Chem. Eng. J. 286 (2016) 223–231.
[26] X. Cheng, H. Guo, Y. Zhang, X. Wu, Y. Liu, Non-photochemical production of singlet oxygen via activation of persulfate by carbon nanotubes, Water Res. 113 (2017) 80–88.
[27] Y. Zhou, J. Jiang, Y. Gao, J. Ma, S.-Y. Pang, J. Li, X.-T. Lu, L.-P. Yuan, Activation of peroxymonosulfate by benzoquinone: a novel nonradical oxidation process, Environ. Sci. Technol. 49 (2015) 12941–12950.
[28] C. Wang, J. Kang, H. Sun, H.M. Ang, M.O. Tadé, S. Wang, One-pot synthesis of N-doped graphene for metal-free advanced oxidation processes, Carbon 102 (2016) 279–287.
[29] P. Liang, C. Zhang, X. Duan, H. Sun, S. Liu, M.O. Tade, S. Wang, An insight into metal organic framework derived N-doped graphene for the oxidative degradation of persistent contaminants: formation mechanism and generation of singlet oxygen from peroxymonosulfate, Environ. Sci. Nano 4 (2017) 315–324.
[30] P. Liang, C. Zhang, X. Duan, H. Sun, S. Liu, M.O. Tade, S. Wang, N-doped graphene from metal-organic frameworks for catalytic oxidation of p-hydroxylbenzoic acid: N-functionality and mechanism, ACS Sustainable Chem. Eng. 5 (2017) 2693–2701.
[31] X. Duan, H. Sun, S. Wang, Metal-free carbocatalysis in advanced oxidation reactions, Acc. Chem. Res. 51 (2018) 678–687.